J|A|C|S
ARTICLES
Published on Web 08/31/2002

Isotope Effects and the Mechanism of an Electron-Transfer-Catalyzed Diels−Alder Reaction

Nicolas J. Saettel,[†] Olaf Wiest,*[,†] Daniel A. Singleton,*[,‡] and Matthew P. Meyer[‡]

Contribution from the Department of Chemistry and Biochemistry, University of Notre Dame, Notre Dame, Indiana 46556-5670, and Department of Chemistry, Texas A&M University, P.O. Box 30012, College Station, Texas 77842

Received May 15, 2002

Abstract: The electron-transfer-catalyzed Diels−Alder reaction of indole and 1,3-cyclohexadiene was studied by a combination of experimental and theoretical methods. The ^{13}C kinetic isotope effects were determined at natural abundance by NMR methodology. B3LYP/6-31G* calculations allow for the first time a quantitatively accurate description of the different possible pathways and provide the basis for an analysis of the experimentally observed isotope effects. The computational results, in conjunction with experimental observations, show that the reaction has a stepwise mechanism that is initiated by attack of the diene into the 3-position of the indole. Numerical simulation of the experimentally observed isotope effects shows that the first step is rate-determining and that the electron exchange in the reactant contributes partially to the overall isotope effect. The combination of electronic structure theory, experimental isotope effects, and numerical simulation thus allows a detailed analysis of a complex reaction mechanism.

Introduction

Novel and unusual modes of reactivity provide the potential for advances in synthetic capability. Mechanistic understanding is key to the rational development of this potential, but a complete mechanistic picture of a complex reaction is often difficult to achieve. An example of novel reactivity has been the advent of electron-transfer-catalyzed cycloadditions, particularly those involving radical cation intermediates. Radical-cation-mediated cycloadditions accomplish a variety of highly regio- and chemoselective transformations while typically increasing rates over the neutral reaction by several orders of magnitude.[1−6] This makes possible sterically hindered or electronically disfavored reactions as well as thermally "forbidden" cycloadditions. These reactions have seen increasing use in complex synthesis.[7]

In simplest form, the mechanism of radical-cation-mediated cycloadditions starts with one of the addends undergoing electron transfer to a one-electron oxidant (eq 1). This redox umpolung process activates the molecule and a cycloaddition ensues. The product is then formed by electron transfer to the cycloadduct radical cation from either another molecule of starting material or the reduced form of the initial oxidant. The kinetics of these reactions have been carefully studied and the basic mechanism is in most cases on solid footing.[8] However, the nature of the stereo- and regioselectivity and reactant selectivity in these reactions is much less well understood. This is in part due to uncertainty over the importance of electron-transfer versus cycloaddition steps in determining products and in part due to a limited understanding of the key cycloaddition step itself.

$$X + Y \xrightarrow{-e^-} X^{+\bullet} + Y \rightarrow XY^{+\bullet} \xrightarrow{+e^-} XY \qquad (1)$$

Experimental studies of the cycloaddition step in these reactions have typically focused on electronic probes to determine which of the addends is oxidized[9] and stereochemical probes to determine the concerted versus stepwise nature of the cycloaddition.[10,11] Several radical-cation-mediated cycloadditions are stereospecific, including the Diels−Alder reactions of

* Address correspondence to this author. E-mail: owiest@nd.edu and singleton@mail.chem.tamu.edu.
[†] University of Notre Dame.
[‡] Texas A&M University.

(1) (a) Bellville, D. J.; Bauld, N. L. *J. Am. Chem. Soc.* **1982**, *104*, 2665. (b) Pabon, R. A.; Bellville, D. J.; Bauld, N. L. *J. Am. Chem. Soc.* **1983**, *105*, 5158. (c) Stufflebeme, G.; Lorenz, K. T.; Bauld, N. L. *J. Am. Chem. Soc.* **1986**, *108*, 4234. (d) Bauld, N. L.; Bellville, D. J.; Harirchian, B.; Lorenz, K. T.; Pabon, R. A., Jr.; Reynolds, D. W.; Wirth, D. D.; Chiou, H. S.; Marsh, B. K. *Acc. Chem. Res.* **1987**, *20*, 371.
(2) (a) Schutte, R.; Freeman, G. R. *J. Am. Chem. Soc.* **1969**, *91*, 3715. (b) Bell, F. A.; Ledwith, A.; Sherrington, D. C. *J. Chem. Soc. C* **1969**, 2719.
(3) (a) Libman, J. *Chem. Commun.* **1976**, 363. (b) Jones, C. R.; Allman, B. J.; Mooring, A.; Spahic, B. *J. Am. Chem. Soc.* **1983**, *105*, 652. (c) Calhoun, G. C.; Schuster, G. B. *J. Am. Chem. Soc.* **1984**, *106*, 6870.
(4) (a) Mattay, J.; Gersdorf, J.; Mertes, J. *J. Chem. Soc., Chem. Commun.* **1985**, 1088. (b) Mattay, J.; Trampe, G.; Runsink, J. *Chem. Ber.* **1988**, *121*, 1991. (c) Mueller, F.; Mattay, J. *Chem. Rev.* **1993**, *93*, 99.
(5) (a) Peglow, T.; Blechert, S.; Steckhan, E. *Chem. Eur. J.* **1998**, *4*, 107. (b) Guertler, C. F.; Blechert, S.; Steckhan, E. *Angew. Chem., Int. Ed. Engl.* **1995**, *34*, 1900. (c) Mlcoch, J.; Steckhan, E. *Angew. Chem.* **1985**, *97*, 429−31. (d) Peglow, T.; Blechert, S.; Steckhan, E. *Chem. Commun.* **1999**, 433.
(6) (a) Schmittel; von Seggern, H. *Angew. Chem., Int. Ed. Engl.* **1991**, *30*, 999. (b) Schmittel, M.; Wöhrle, C. *J. Org. Chem.* **1995**, *60*, 8223.
(7) (a) Harirchian, B.; Bauld, N. L. *J. Am. Chem. Soc.* **1989**, *111*, 1826. (b) Rossler, U.; Blechert, S.; Steckhan, E. *Tetrahedron Lett.* **1999**, *40*, 7075. (c) Jacobi, P. A.; Lee, K. *J. Am. Chem. Soc.* **1997**, *119*, 3409. (d) Kadota, S.; Tsubono, K.; Makino, K.; Takeshita, M.; Kikuchi, T. *Tetrahedron Lett.* **1987**, *28*, 2857.
(8) (a) Lorenz, K. T.; Bauld, N. L. *J. Am. Chem. Soc.* **1987**, *109*, 1157. (b) Reynolds, D. W.; Lorenz, K. T.; Chiou, H. S.; Bellville, D. J.; Pabon, R. A.; Bauld, N. L. *J. Am. Chem. Soc.* **1987**, *109*, 4960. (c) See also: Gassman, P. G.; Singleton, D. A. *J. Am. Chem. Soc.* **1984**, *106*, 7993.
(9) (a) Chockalingam, K.; Pinto, M.; Bauld, N. L. *J. Am. Chem. Soc.* **1990**, *112*, 447. (b) Mlcoch, J.; Steckhan, E. *Tetrahedron Lett.* **1987**, *28*, 1081.
(10) Wiest, O.; Steckhan, E. *Tetrahedron Lett.* **1993**, *34*, 6391.
(11) (a) Bauld, N. L.; Gao, D. *J. Chem. Soc., Perkin Trans. 2* **2000**, 191. (b) Bauld, N. L.; Yang, J.; Gao, D. *J. Chem. Soc., Perkin Trans. 2* **2000**, 207.

10.1021/ja026924z CCC: $22.00

cyclohexadiene with 2,4-hexadiene and cyclopentadiene with *trans*-anethole and *cis*- and *trans*-diaryloxyethenes, along with the [2 + 2] dimerization of *trans*- and *cis*-anetholes.[12,13] On the other hand, the radical-cation-mediated Diels−Alder reactions of cyclopentadiene with *cis*- and *trans*-propenyl ethers, vinylanisole, *cis*-anethole, and N-vinylcarbazole, as well as the [2 + 2] dimerization of N-vinylcarbazole, are all nonstereospecific.[11,12,14] In such reactions, the cycloaddition must occur at least partially by a stepwise process, and acyclic intermediates have been detected in some cases.[15] Complicating the interpretation is a substantial "memory" effect among the nonstereospecific reactions—isomeric alkenes do not afford the same product mixtures. These observations suggest that ring closure in a stepwise process can compete well with loss of stereochemistry by bond rotation. In addition, stereospecific Diels−Alder adducts can potentially be formed by an initial [2 + 2] cycloaddition followed by an electron-transfer-catalyzed [1,3] methylene shift.[16] Thus, it is by no means clear that the stereospecific reactions involve concerted cycloadditions.[14]

Theoretical studies of radical-cation-mediated cycloadditions have focused on very simple models.[17−19] Recent DFT and highly correlated MO calculations have studied the radical cation Diels−Alder reactions of 1,3-butadiene radical cation with ethene[20−22] or acetylene.[23] These calculations predict a stepwise cycloaddition starting from one of several possible ion−molecule complexes. Formation of one C−C bond gives an acyclic intermediate that closely resembles the corresponding biradical in a neutral stepwise Diels−Alder reaction.[24] This intermediate is in an ~1.5 kcal/mol well on the potential energy hypersurface and may either consummate the Diels−Alder reaction or undergo bond rotation and ring closure to lead to a vinylcyclobutane product. Similar intermediates were found in semiempirical and DFT calculations of radical cation Diels−Alder reactions of indoles.[25] These calculations also demonstrate a well-known property of many radical cation hypersurfaces, that is, their extraordinary flatness.[26,27] Since most transition structures and intermediates on these surfaces are within a few kcal/mol of each other, even the relatively small error of modern computational methods is often sufficient to change the rate-determining step of a multistep reaction or to yield spurious minima on the hypersurface that disappear when reinvestigated at higher levels.[20−22] This behavior often complicates the interpretation of the computational results.

We describe here a combined experimental and theoretical study of a complex and synthetically useful radical-cation-mediated Diels−Alder reaction. This includes the characterization of the mechanism by kinetic isotope effects (KIEs), which presents some novel challenges because of the interleaving of chemical and electron-transfer steps. Neither experiment nor theory by itself defines the mechanism. Together, the results delineate the cycloaddition pathway and the product-determining step in this reaction and provide broad insight on selectivity in radical-cation-mediated cycloadditions.

Results and Discussion

Choice of System. Mostly simple hydrocarbons were used in radical cation Diels−Alder reactions[28] until Steckhan found that indole (**2**) is an excellent dienophile in photochemically induced electron-transfer reactions catalyzed by triarylpyrylium salts.[29] Aside from its interest as a nontrivial reaction, this system exhibits a defined pattern of complete regioselectivity—1-substituted dienes (**1a**) afford 1-substituted tetrahydrocarbazols (**3a**) while 2-substituted dienes (**1b**) afford 3-substituted tetrahydrocarbazols (**3b**) (eq 2). Another advantage for mechanistic study is that there is no ambiguity (vide infra) in the identity of the reactive cation radical. The radical cation Diels−Alder reaction of **2** with 1,3-cyclohexadiene was chosen in particular because it cleanly affords cycloadducts in high yield.

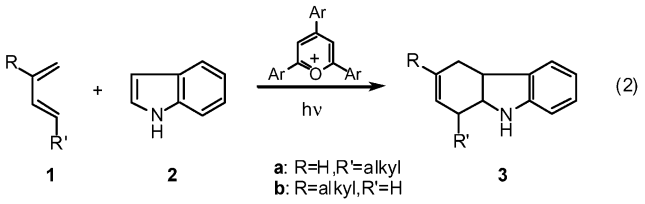

(2)

Isotope Effects. As previously described,[29] reactions of **2** with cyclohexadiene were run in the presence of acetyl chloride and $NaHCO_3$. These conditions trap the initial endo and exo cycloadducts **4** and **5** as the acetamides **6** and **7** as shown in Scheme 1. This acetylation raises the oxidation potential of the adducts, which is necessary because they are more easily oxidized than the starting **2** and inhibit the cycloaddition. The starting **2** is not acetylated under these conditions. The cycloaddition is associated with the presence of aminium ion catalyst and no significant reaction occurred after the blue color of the aminium catalyst faded.

The complete set of ^{13}C KIEs for **2** in this reaction was determined combinatorially at natural abundance by NMR methodology.[30] Two reactions of **2** with a 2-fold excess of cyclohexadiene catalyzed by tris(4-bromophenyl)aminium hexachloroantimonate were carried out on a 0.43 mol scale and taken to 75.6 ± 1.4% and 78.9 ± 1.5% conversion. After quenching with sodium ethoxide in ethanol and an aqueous workup, the unreacted **2** was chromatographically reisolated and analyzed by ^{13}C NMR compared to a standard sample of the original **2**. The relative

(12) (a) Bauld, N. L.; Gao, D. *J. Chem. Soc., Perkin Trans. 2* **2000**, 931. (b) Bauld, N. L.; Yang, J. *Org. Lett.* **1999**, *1*, 773.
(13) Bauld, N. L.; Pabon, R. *J. Am. Chem. Soc.* **1983**, *105*, 633.
(14) (a) Gao, D.; Bauld, N. L. *J. Org. Chem.* **2000**, *65*, 6276. (b) Bauld, N. L.; Yang, J. *Tetrahedron Lett.* **1987**, *40*, 8519.
(15) (a) Roth, H. D.; Schilling, M. L. M. *J. Am. Chem. Soc.* **1985**, *107*, 716. (b) Turececk, F.; Hanus, V. *Mass Spectrom. Rev.* **1984**, *3*, 85.
(16) (a) Pabon, R. A.; Bellville, D. J.; Bauld, N. L. *J. Am. Chem. Soc.* **1984**, *106*, 2730. (b) Botzem, J.; Haberl, U.; Steckhan, E.; Blechert, S. *Acta Chem. Scand.* **1998**, *52*, 175.
(17) Bellville, D. J.; Bauld, N. L. *Tetrahedron* **1986**, *42*, 6167.
(18) Schmittel, M.; Wohrle, C.; Bohn, I. *Acta Chem. Scand.* **1997**, *51*, 151.
(19) Bauld, N. L. *J. Am. Chem. Soc.* **1992**, *114*, 5800.
(20) Hofmann, M.; Schaefer, H. F., III. *J. Am. Chem. Soc.* **1999**, *121*, 6719.
(21) Haberl, U.; Wiest, O.; Steckhan, E. *J. Am. Chem. Soc.* **1999**, *121*, 6730.
(22) Hofmann, M.; Schaefer, H. F., III. *J. Phys. Chem. A* **1999**, *103*, 8895.
(23) Bouchoux, G.; Nguyen, M. T.; Salpin, J.-Y. *J. Phys. Chem. A* **2000**, *104*, 5778.
(24) (a) Goldstein, E.; Beno, B.; Houk, K. N. *J. Am. Chem. Soc.* **1996**, *118*, 6036. (b) Beno, B. R.; Houk, K. N.; Singleton, D. A. *J. Am. Chem. Soc.* **1996**, *118*, 9984.
(25) (a) Wiest, O.; Steckhan, E.; Grein, F. *J. Org. Chem.* **1992**, *57*, 4034. (b) Haberl, U.; Steckhan, E.; Blechert, S.; Wiest, O. *Chem. Eur. J.* **1999**, *5*, 2859.
(26) Sastry, G. N.; Bally, T.; Hrouda, V.; Carsky, P. *J. Am. Chem. Soc.* **1998**, *120*, 9323.
(27) (a) Saettel, N. J.; Oxgaard, J.; Wiest, O. *Eur. J. Org. Chem.* **2001**, 1429. (b) Bally, T.; Borden, W. T. In *Reviews in Computational Chemistry*; Lipkowitz, K. B., Boyd., D. B., Eds.; Wiley & Sons: New York, 1999; Vol. 13, p 1.
(28) For some radical cation Diels−Alder reactions containing heterosubstituted dienes or dienophiles, compare: Bauld, N. L.; Harirchian, B.; Reynolds, D. W.; White, J. C. *J. Am. Chem. Soc.* **1988**, *110*, 8111; and ref 1b.
(29) (a) Gieseler, A.; Steckhan, E.; Wiest, O. *Synlett* **1990**, 275. (b) Gieseler, A.; Steckhan, E.; Wiest, O.; Knoch, F. *J. Org. Chem.* **1991**, *56*, 1405.
(30) Singleton, D. A.; Thomas, A. A. *J. Am. Chem. Soc.* **1995**, *117*, 9357.

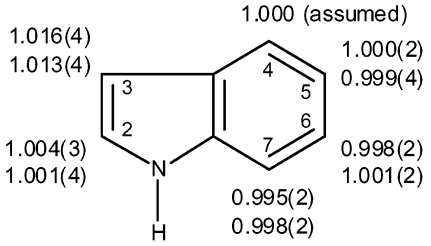

Figure 1. ^{13}C KIEs (0 °C) for the radical-cation-catalyzed Diels−Alder reaction of **2** with cyclohexadiene.

Scheme 1

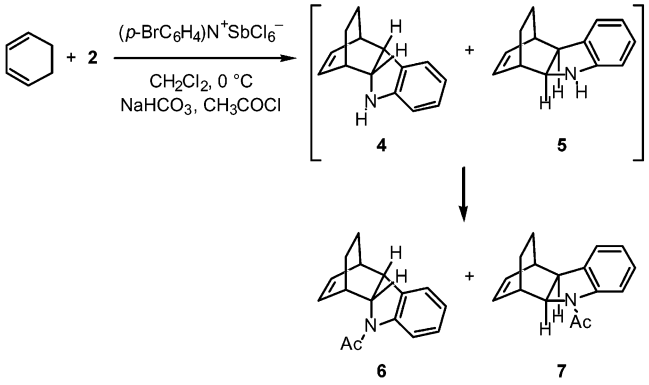

changes in ^{13}C composition were calculated using C4 as an internal standard with the assumption that its isotopic composition did not change. From the changes in isotope composition, the isotope effects were calculated as previously described.[30] The results are summarized in Figure 1. Consistent integrations were not obtainable for the sharp, slow-relaxing quaternary carbons, and KIEs were not calculated for these positions.

Qualitatively, the significant ^{13}C KIE at C3 indicates that a new bond is being formed to C3 in the rate-limiting step of the cycloaddition. The low ^{13}C KIE at C2 does not rule out a highly asynchronous concerted cycloaddition, but the results are readily consistent with a stepwise process. For a stepwise cycloaddition, the KIEs cannot qualitatively distinguish between initial rate-limiting bond formation to C3 or initial bond formation to C2 followed by rate-limiting ring closure at C3. However, the KIEs would normally be interpreted as ruling out rate-limiting attack or ring closure at C2.

Theoretical Studies. Four reaction pathways were investigated in B3LYP calculations employing a 6-31G* basis set, varying by whether the endo or exo product is formed and by whether initial bond formation is to C2 or C3 of **2**. Starting with an initial "supermolecule" of cyclohexadiene and **2** at a large (20 Å) separation (**8**), ionization leads to the ion−molecule complex $\mathbf{8}^{\bullet+}$ with an adiabatic ionization energy of 155 kcal/mol. The distances in $\mathbf{8}^{\bullet+}$ from C2 and C3 of the indole to the closest carbon in cyclohexadiene are 3.29 and 4.49 Å, respectively. A second ion−molecule complex of virtually identical energy was also located where these distances are 4.69 and 3.21 Å, respectively. Presumably, other loose complexes could be located, and the structures are likely to be fluctional in nature.[21] The complex $\mathbf{8}^{\bullet+}$ is predicted to be 15 kcal/mol lower in energy than separate cyclohexadiene and $\mathbf{2}^{\bullet+}$, but after allowance for entropy and solvation effects, these complexes are likely to exist in only very shallow wells on the free-energy surface in solution.

Initial bond formation at C3 of $\mathbf{2}^{\bullet+}$ ("C3-attack") can lead to two diastereomeric intermediates that ultimately afford endo and exo products. The calculated pathways for formation of these products are shown in Figures 2 and 3, respectively.

The first-step transition structure *endo*-$\mathbf{9}^{\bullet+}$ is 6.6 kcal/mol higher in energy than $\mathbf{8}^{\bullet+}$. The forming C3−C1′ bond length of 2.10 Å would be typical for a concerted Diels−Alder reaction but is relatively long for a stepwise cycloaddition. This is most likely due to the radical cationic character of $\mathbf{1}^{\bullet+}$ since the forming bond represents the HOMO.[21] The *endo*-$\mathbf{9}^{\bullet+}$ leads to the intermediate *endo*-$\mathbf{10}^{\bullet+}$, where the new C3−C1′ bond is fully formed at 1.61 Å. In this structure, the cation is stabilized as an iminium cation and delocalized over the pyrrole moiety as

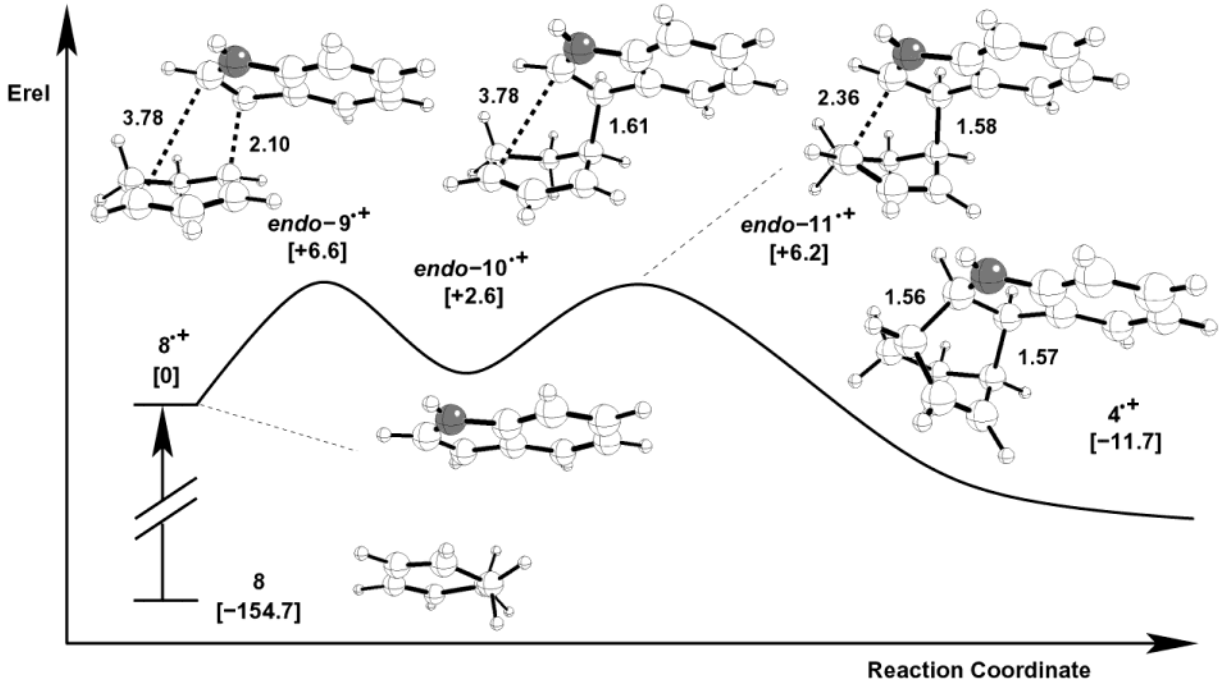

Figure 2. Calculated pathway for formation of the endo product starting with C3-attack. Energies are B3LYP/6-31G* +zpe in kcal/mol relative to $\mathbf{8}^{\bullet+}$.

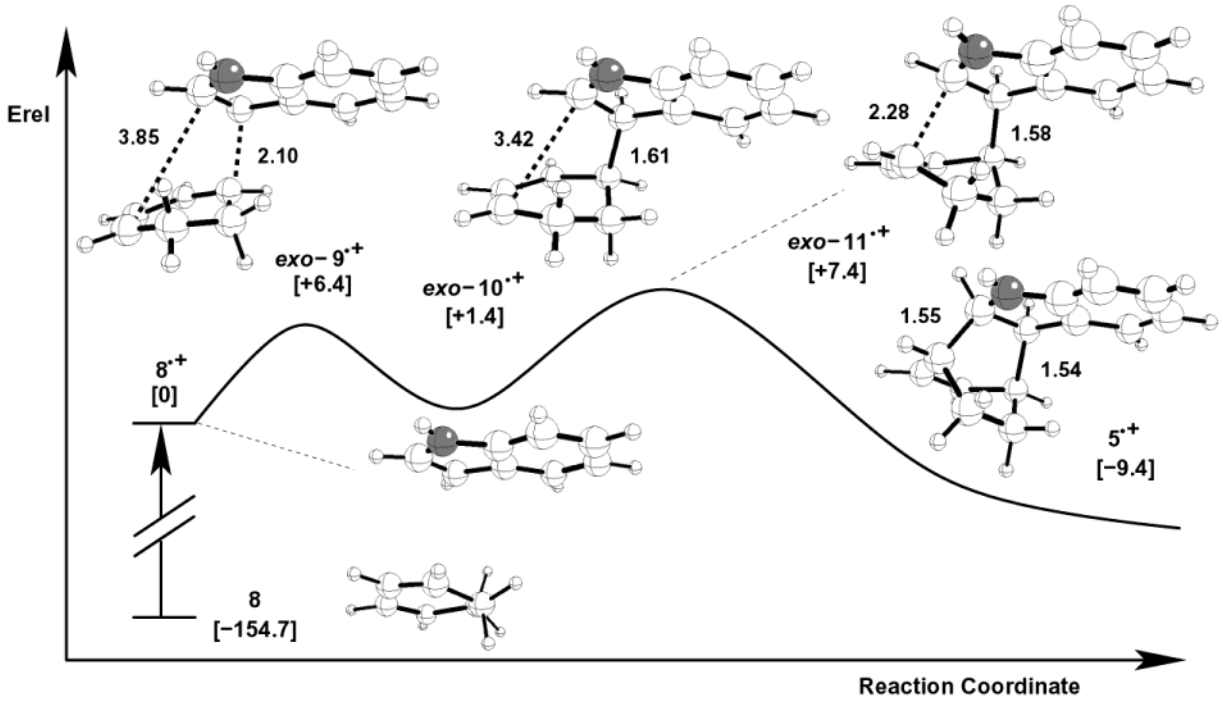

Figure 3. Calculated pathway for formation of the exo product starting with C3-attack. Energies are B3LYP/6-31G* +zpe in kcal/mol relative to **8**•+.

shown from the Mulliken charges in Figure 4, whereas the radical character is localized as an allyl radical in the diene moiety of the cyclohexadiene as shown from the spin densities. The *endo*-**10**•+ appears strongly stabilized but so was the initial **8**•+, so the formation of *endo*-**10**•+ is still endothermic by 2.6 kcal/mol higher relative to **8**•+. The second-step transition structure *endo*-**11**•+ has a relative energy of 6.2 kcal/mol and is only slightly lower in energy than *endo*-**9**•+. Because of the 9.2 kcal/mol exothermic reaction step from *endo*-**10**•+ to **4**•+, the forming C2−C4′ bond in *endo*-**11**•+ is, at 2.36 Å, quite long, as is to be expected from an early transition state. The overall reaction energy of −11.7 kcal/mol is considerably less exothermic than the neutral reaction. This is due to the weaker stabilization of the radical cation character in **4**•+ compared to **8**•+.

The corresponding exo intermediates and transition structures in Figure 3 are quite similar to the endo structures, with calculated forming bond lengths that are virtually identical. However, there are some significant differences in the energetics of this reaction pathway. The overall reaction energy of −9.4 kcal/mol is 2.3 kcal/mol less exothermic than the endo pathway. This is due to a steric repulsion between the hydrogens on the saturated bridge of the cyclohexadiene moiety and the indole ring, with H/C and H/N contact distances as low as 2.6 Å. This incipient steric interaction raises the energy of the second-step transition structure *exo*-**11**•+ to where the second step becomes rate-limiting in the exo pathway. As a result, the endo product is favored despite *exo*-**9**•+ and *exo*-**10**•+ being favored over *endo*-**9**•+ and *endo*-**10**•+!

Though the exact agreement might possibly be fortuitous, the difference in activation energies between the endo and exo C3-attack pathways of 0.8 kcal/mol corresponds very well with the experimentally observed 3:1 ratio (=0.6 kcal/mol at 273 K, assuming equal entropies of activation) of products.

Because indole preferentially undergoes electrophilic aromatic substitution at C3, qualitative considerations suggest that the

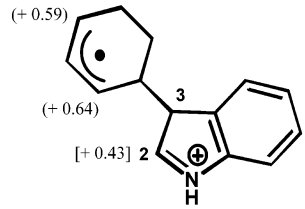

Figure 4. Intermediate **10**•+ resulting from a C3-attack. Spin densities are given in parentheses and Mulliken charges with hydrogen summed into heavy atoms are given in brackets.

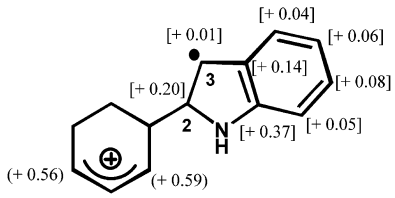

Figure 5. Intermediate **13**•+ resulting from a C2-attack. Spin densities are given in parentheses and Mulliken charges with hydrogen summed into heavy atoms are given in brackets.

intermediate **10**•+ from C3 attack ought to be more stable than the intermediate **13**•+ (Figure 5) resulting from initial bond formation at C2 of **2** ("C2-attack"). Low-level calculations have supported this idea.[25a] However, the first-step transition state for these cycloadditions is relatively early and the influence of a communicative incipient allylic radical at the transition state for C2-attack is hard to anticipate. It is therefore difficult to be certain a priori whether C3-attack or C2-attack would be favored.

Figures 6 and 7 summarize the calculated pathways for endo and exo C2-attack, respectively. Interestingly, for both C2-attack cycloadditions, the second step is predicted to be rate-limiting. For C2-attack, the endo product is correctly favored, but the predicted preference of 1.4 kcal/mol (comparing *endo*-**14**•+ with *exo*-**14**•+) is not as close to experiment as was seen with the

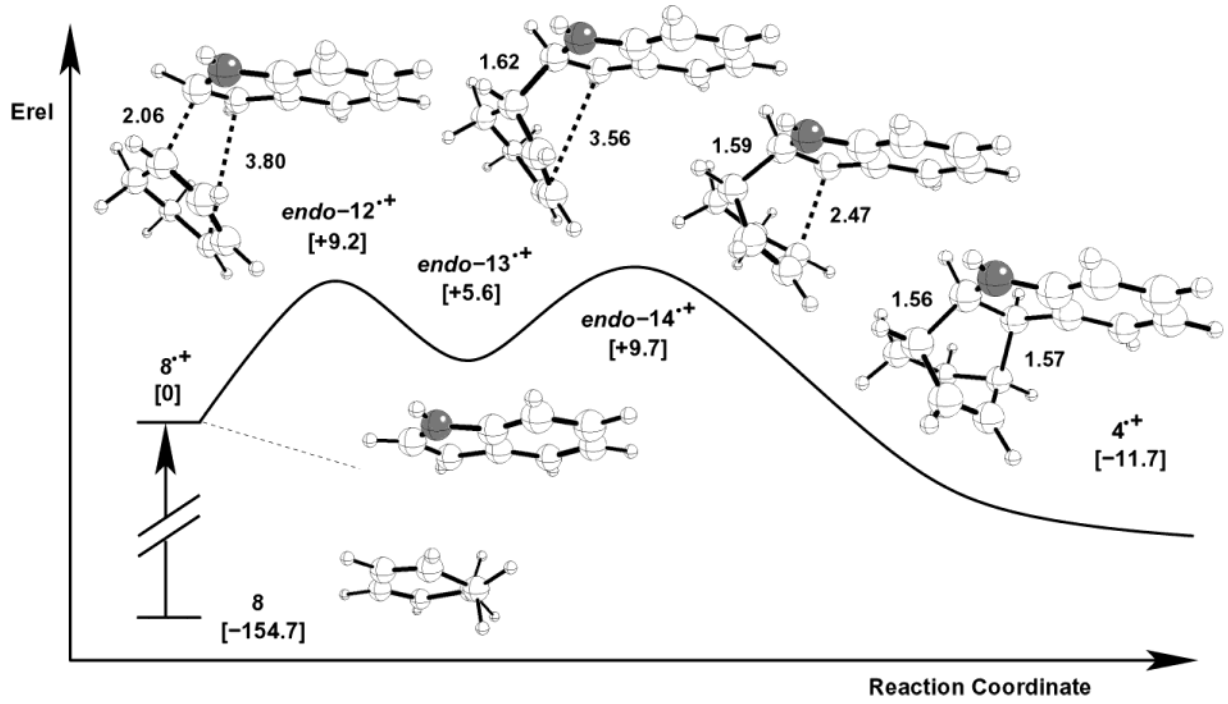

Figure 6. Calculated pathway for formation of the endo product starting with C2-attack. Energies are B3LYP/6-31G* +zpe in kcal/mol relative to **8**•+.

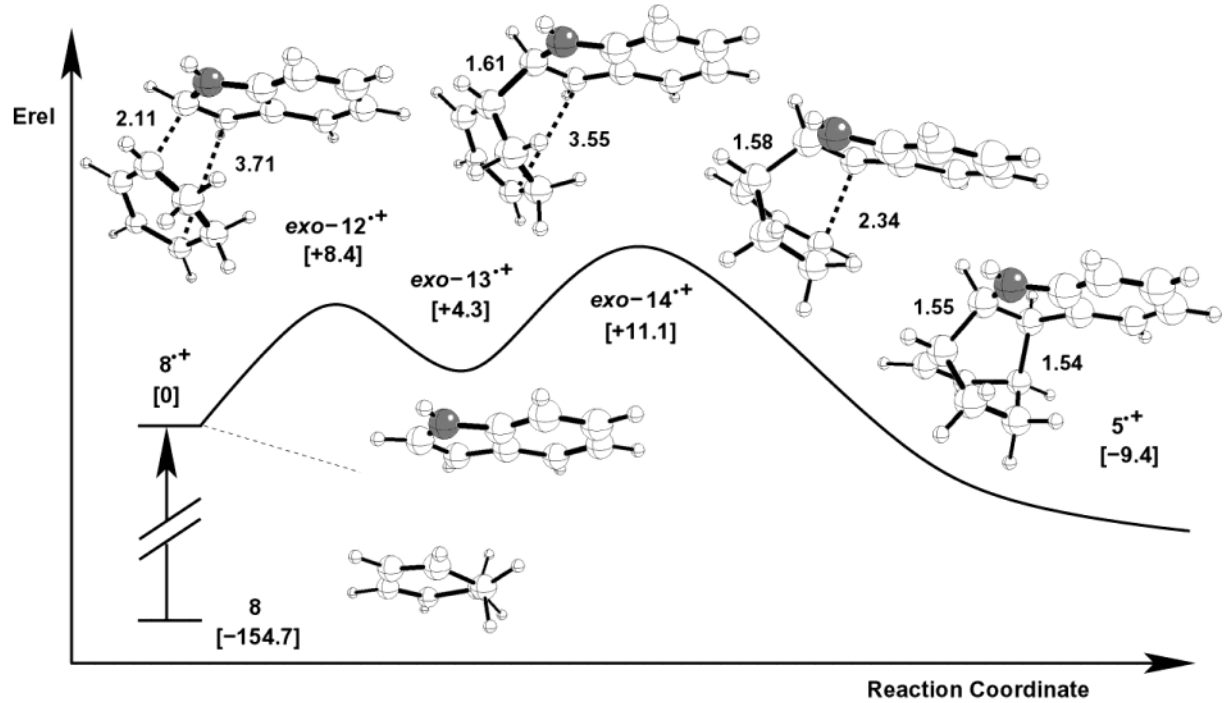

Figure 7. Calculated pathway for formation of the exo product starting with C2-attack. Energies are B3LYP/6-31G* +zpe in kcal/mol relative to **8**•+.

C3-attack results. Both C2-attack pathways are predicted to be significantly disfavored, by ∼3−4 kcal/mol, relative to the C3-attack pathways.

There are several arguments against the viability of the C2-attack pathways. First, the calculated energy difference between the C2- and C3-attack pathways is large compared to the error that can reasonably be expected for the methodology used. Considering the similarity of the species involved and the resulting cancellation of any systematic bias of the B3LYP method, it is unlikely that the calculational errors are large enough for the C2 pathway to be correct. Second, the C2 pathway is very weak in its prediction of the experimental endo/exo ratio, unlike the prediction for the C3 pathway. Finally, it would be very difficult to reconcile the regiochemistry of reactions of unsymmetrical dienes in eq 2 with a C2-attack pathway.[25,29] Our conclusion is that the pathways involving a C2-attack can be excluded.

The theoretical calculations by themselves still leave some important questions unresolved, even when interpreted in a most credulous light. The calculations obviously cannot address the issue of whether reactant selectivity is determined in an electron-transfer or a cycloaddition step. An equally important but subtler issue is the question of the rate-limiting step. The energies for

$\mathbf{9}^{\bullet+}$ and $\mathbf{11}^{\bullet+}$ do not allow for entropy or solvent effects. Entropy might be expected to raise the barrier for the more organized $\mathbf{11}^{\bullet+}$ over that for the looser $\mathbf{9}^{\bullet+}$. On the other hand, the charge is less delocalized in $\mathbf{11}^{\bullet+}$ and allowance for solvent stabilization will lower the relative barrier for $\mathbf{11}^{\bullet+}$. Either of these effects may be calculationally addressed,[25] but probably not with an accuracy that can reliably distinguish the rate-limiting step among closely competitive barriers. Analysis of the isotope effects addresses these issues.

Kinetic Models and Predicted KIEs. One idea behind the combined use of experimental isotope effects and theoretical calculations is to use the theory to interpret the KIEs and conversely use the experimental KIEs to validate the theoretical predictions. This requires a prediction of ^{13}C KIEs from the theoretical calculations, often a simple matter. Such predictions have been highly successful for reactions not involving hydrogen transfer.[31] The prediction of KIEs here, however, is complicated by a multistep mechanism involving high rates of both electron-transfer and chemical conversions. Under the circumstances, a kinetic model is required for KIE predictions.

One very simplified model is that of eq 3. We first consider the limiting case where $k_2 \gg k_{-1}$. In this case, the isotope effects observed would be those for oxidation of **2**. If this oxidation is exothermic in a range where k_1 is diffusion controlled, then KIEs of unity would be expected. If **2**'s oxidation is endothermic, diffusion apart of $\mathbf{2}^{\bullet+}$ from reduced oxidant will likely control k_1. The KIEs would then reflect the equilibrium isotope effect for formation of $\mathbf{2}^{\bullet+}$ from **2**. The predicted equilibrium KIEs (see Experimental for details) are shown in Table 1 and they do not fit with experiment. By itself, this analysis allows the significant conclusion that electron transfer to form $\mathbf{2}^{\bullet+}$ is at least partially reversible. Thus, starting material reactivity depends on the reactivity of the intermediate radical cation and not just on its ease of formation.

$$\mathbf{2} \underset{k_{-1}}{\overset{k_1}{\rightleftharpoons}} \mathbf{2}^{\bullet+} \xrightarrow{k_2} \text{products} \qquad (3)$$

The opposite limiting case is where formation of $\mathbf{2}^{\bullet+}$ is rapidly reversible ($k_2 \ll k_{-1}$). As long as the concentration of $\mathbf{2}^{\bullet+}$ is small compared to **2**, the isotope effect will just be the multiple of the equilibrium isotope effect for the oxidation and the kinetic isotope effect for the cycloaddition. For a qualitative interpretation of the experimental KIEs, it may be assumed that the equilibrium isotope effects are small and that a significant ^{13}C KIE results when a carbon gains a bonded atom in the rate-limiting step. Having excluded C2-attack above, the observation of a significant C3 KIE and little C2 KIE is qualitatively indicative of a rate-limiting first step for C3-attack.

The theoretically predicted isotope effects for endo C3-attack for this kinetic model (Table 1) support the qualitative interpretation. If the second-step transition structure *endo*-$\mathbf{11}^{\bullet+}$ were rate-limiting, the calculations would predict KIEs that run quite counter to the experimental values. However, for a rate-limiting first-step transition structure *endo*-$\mathbf{9}^{\bullet+}$, the calculations correctly predict a substantial isotope effect at C3 and a very small C2 KIE. A 3:1 weighting of *endo*-$\mathbf{9}^{\bullet+}$:*exo*-$\mathbf{11}^{\bullet+}$, on the basis of the experimental product ratio and the theoretically predicted rate-limiting steps, reproduces the pattern of KIEs observed experimentally. Quantitatively, however, this prediction is not impressive because it substantially over-predicts the isotope effect at C3.

A more realistic kinetic model leads to more accurate KIE predictions. A differential kinetic model for these reactions was developed computationally on the basis of eqs 4−8. For this model, oxidation of **2** by the catalytic aminium salt (eq 4), which is highly exothermic, was assumed to be diffusion controlled ($k_1 = 10^{10}$ M^{-1} s^{-1}) and irreversible. The formation of the complex $\mathbf{8}^{\bullet+}$ from $\mathbf{2}^{\bullet+}$ (eq 5) was also assumed to be diffusion controlled, and for the high concentrations of cyclohexadiene present this is too fast to be of consequence. The rate of formation of the product cation radical $\mathbf{4}^{\bullet+}$ (or $\mathbf{5}^{\bullet+}$) from $\mathbf{8}^{\bullet+}$ (eq 6) was varied to examine the effect of k_3 on the isotope effects. The rate of oxidation of **2** by $\mathbf{4}^{\bullet+}$ and its potential reversibility (ignored here) affect the overall rate of reaction but are not critical to the KIE prediction. The exchange of indole molecules between free **2** and complex $\mathbf{8}^{\bullet+}$ (eq 8) is significant when one of the molecules contains a ^{13}C, and k_5 was also varied to examine its impact of the isotope effects. Separate equations in the model were applied to both unlabeled and ^{13}C-containing materials, with k_3 adjusted by the theoretically predicted KIE and with k_4 and k_{-5} adjusted to give the theoretically predicted equilibrium isotope effects. Rate constants k_1, k_2, and k_4 were assumed to be isotope-independent.

$$Ar_3N^{\bullet+} + \mathbf{2} \xrightarrow{k_1} Ar_3N + \mathbf{2}^{\bullet+} \qquad (4)$$


$$+ \mathbf{2}^{\bullet+} \xrightarrow{k_2} \mathbf{8}^{\bullet+} \qquad (5)$$

$$\mathbf{8}^{\bullet+} \xrightarrow{k_3} \mathbf{4}^{\bullet+} \qquad (6)$$

$$\mathbf{4}^{\bullet+} + \mathbf{2} \xrightarrow{k_4} \mathbf{4} + \mathbf{2}^{\bullet+} \qquad (7)$$

$$\mathbf{8}_{12C}{}^{\bullet+} + \mathbf{2}_{13C} \underset{k_{-5}}{\overset{k_5}{\rightleftharpoons}} \mathbf{2}_{12C} + \mathbf{8}_{13C}{}^{\bullet+} \qquad (8)$$

Isotope effects were calculated for this model by numerically integrating the kinetic equations, starting with reactant concentrations that approximate the experimental conditions. (See Supporting Information for the computational program.) The most striking outcome from this simulation is that it is very difficult for k_5, the electron exchange of eq 8, to be fast enough to see the full limiting-case isotope effect obtained from eq 3. For example, if k_5 is as fast as 10^9 M^{-1} s^{-1} and k_3 is 10^7 s^{-1}, only 90% of the cycloaddition isotope effect on k_3 would be detected experimentally. If k_5 is reduced to 10^8 M^{-1} s^{-1}, only about half of the cycloaddition isotope effect would be observed. Any prediction of KIEs depends on an uncertain estimate of k_3 and k_5, but under a variety of reasonable kinetic possibilities, the predicted KIEs would approximate those observed experimentally. For example, using $k_5 = 10^8$ M^{-1} s^{-1} and $k_3 = 10^7$ s^{-1}, the predicted KIEs from the last column of Table 1 are reduced to 1.003, 1.014, 0.999, 0.999, and 0.999 for C2, C3, C5, C6, and C7, respectively. This reproduces the experimental KIEs well. This exercise in numerology does not allow us to extract definitive values for the rates of electron exchange, k_5, and cycloaddition, k_3. How-

(31) Meyer, M. P.; DelMonte, A. J.; Singleton, D. A. *J. Am. Chem. Soc.* **1999**, *121*, 10865.

Table 1. Calculated Isotope Effects for the Model of Eq 3

		$k_2 \gg k_{-1}$					
position	$k_2 \gg k_{-1}$	*endo*-**9**$^{\bullet+}$	*endo*-**11**$^{\bullet+}$	*exo*-**9**$^{\bullet+}$	*exo*-**11**$^{\bullet+}$	3:1 *endo*-**9**$^{\bullet+}$: *exo*-**11**$^{\bullet+}$	experimental
C2	0.994	0.998	1.023	0.999	1.026	1.005	1.001−1.004
C3	0.999	1.034	1.000	1.035	1.000	1.026	1.013−1.016
C4	1[a]	1[a]	1[a]	1[a]	1[a]	1[a]	1
C5	1.000	0.998	0.999	0.998	0.999	0.999	0.999−1.000
C6	0.997	0.998	0.999	0.998	0.999	0.998	0.998−1.001
C7	0.995	0.999	0.999	0.999	0.999	0.999	0.995−0.998

[a] Because the experimental KIEs are relative to the KIE at C4, all of the predicted KIEs are made relative to C4.

ever, it does show that both steps need to be considered to achieve consistency between the experimental and calculational results.

Regardless of the kinetic uncertainties, the experimental KIEs allow a decision on just those issues that were left unclear by the theoretical calculations. The significant ^{13}C KIE at C3 shows that reactant selectivity is not determined solely in the electron-transfer step, and that, at least for major endo reaction pathway, the initial carbon−carbon bond-forming step is rate-limiting.

Conclusions

The electron-transfer-catalyzed Diels−Alder reaction of indole and 1,3-cyclohexadiene proceeds via formation of an ion−molecule complex, followed by endo attack of the 1,3-cyclohexadiene into the C3-position of the indole radical cation. The transition structure for this first step is rate-limiting and leads to the formation of a singly linked intermediate. This then collapses to the final product via a second transition structure that is only slightly lower in energy. The corresponding exo attack barrier is 0.8 kcal/mol higher in energy, consistent with the experimentally observed endo/exo ration of 3:1. In the exo pathway, the second step is computed to be rate-limiting. The endo selectivity occurs despite the exo pathway being favored in the first step, owing to steric interactions that inhibit the ring-closure step and makes it rate-limiting.

The study presented here demonstrates how theory and experiment can complement each other in the analysis of a complex reaction mechanism. While the experimentally observed isotope effects alone are not able to distinguish the two possible modes of attack into the C2- and C3-positions of the indole, the accuracy of the computational methods, combined with the validation by the experimentally observed endo/exo ratio, is able to exclude the attack in 2-position. In turn, numerical simulations of the isotope effects based on computed force constants and comparison with experimental values are able to determine which of the two transition states is rate-determining. This information could not be obtained reliably on the basis of computational work alone because of the close energetic proximity of the stationary points involved. The synergy between the different approaches thus allows the complete analysis of multiple competing pathways leading to different stereoisomeric products. This approach is therefore also promising for the investigation of similarly complex electron-transfer-induced reactions, thus providing a new tool for the study of radical ionic reaction mechanisms.

Experimental Section

Theoretical Methods. All structures reported here are fully optimized with the Gaussian98 series of programs,[32] employing the B3LYP/6-31G* method which has been shown to yield accurate results for the calculation of hydrocarbon radical cations.[33] Each stationary point has been characterized by a harmonic frequency analysis and each shows the correct number of negative eigenvalues. All energies include a zero-point energy correction.

Table 2. ^{13}C Integrations of Indole and R/R_0's for Radical-Cation-Catalyzed Diels−Alder Additions of 1,3-Cyclohexadiene to Indole

	C2	C3	C4	C5	C6	C7
			expt. 1			
75.6(1.4) %	1000.0	1006.3	1000	999.6	984.1	988.9
Standard	993.7	986.7	1000	999.6	994.5	993.0
R/R_0	1.006	1.022	1.000	1.000	0.994	0.993
$\Delta R/R_0$	0.004	0.006		0.003	0.004	0.003
			expt. 2			
78.9(1.5) %	994.8	1005.9	1000	997.7	991.0	994.1
Standard	993.7	986.7	1000	999.6	994.5	993.0
R/R_0	1.001	1.019	1.000	0.998	0.997	1.001
$\Delta R/R_0$	0.007	0.007		0.006	0.003	0.002

Equilibrium isotope effects were calculated from the analytical frequencies by the method of Biegeleisen and Mayer.[34] The calculations used the program QUIVER[35] with frequencies scaled by 0.9614.[36] Kinetic isotope effect calculations included an infinite parabolic tunneling correction.[37] As a final step, all predicted isotope effects for indole were made relative to the C4 isotope effect for comparison with the relative experimental values.

Cycloaddition of 1,3-Cyclohexadiene with Indole. A mixture of 40.7 mL (34.2 g, 0.427 mol) of freshly distilled 1,3-cyclohexadiene, 25.0 g (0.213 mol) of indole, 15.15 mL (16.73 g, 0.213 mol) of freshly distilled acetyl chloride, 17.92 g (0.213 mol) of powdered sodium bicarbonate, and 8.14 mL (5.94 g, 41.7 mmol) of decane (internal standard) was prepared in 800 mL of CH_2Cl_2 and cooled to 0 °C. To this mixture was added 1.2-g (1.5 mmol) portions of tris(4-bromophenyl)aminium hexachloroantimonate at 1 h intervals. A 0.5-mL aliquot was removed 30 min after each addition of the aminium salt and quenched by addition to 1 mL of saturated sodium ethoxide in ethanol. After partitioning of the resulting mixture between water and CH_2Cl_2, the organic layer was dried (K_2CO_3) and analyzed by GC. After 5 additions of the aminium salt (total of 6 g or 7.5 mmol), the conversion was 75.6 ± 1.4%. The reaction mixture was then quenched by the addition of 800 mL of saturated sodium ethoxide in ethanol. The resulting mixture was rinsed twice with 2 L of water and once with 2 L of brine, and the combined aqueous layers were back-extracted with 400 mL of chloroform. The combined organic layers were dried (Na_2SO_4) and concentrated to 200 mL on a rotary evaporator. The resulting brown-black solution was subjected to a rough chromatography in two portions on a 3″ × 10″ silica gel column using 140:60:1 chloroform/hexanes/tributylamine as eluent. Fractions containing indole were rechromatographed in two portions on a 2″ × 12″ silica gel column using the same eluent to afford 4.0 g of recovered indole (>98% pure, contaminated with traces of tributylamine).

(32) Frisch, M. J.; Trucks, G. W.; Schlegel, H. B.; Scuseria, G. E.; Robb, M. A.; Cheeseman, J. R.; Zakrzewski, V. G.; Montgomery, J. A., Jr.; Stratmann, R. E.; Burant, J. C.; Dapprich, S.; Millam, J. M.; Daniels, A. D.; Kudin, K. N.; Strain, M. C.; Farkas, O.; Tomasi, J.; Barone, V.; Cossi, M.; Cammi, R.; Mennucci, B.; Pomelli, C.; Adamo, C.; Clifford, S.; Ochterski, J.; Petersson, G. A.; Ayala, P. Y.; Cui, Q.; Morokuma, K.; Malick, D. K.; Rabuck, A. D.; Raghavachari, K.; Foresman, J. B.; Cioslowski, J.; Ortiz, J. V.; Baboul, A. G.; Stefanov, B. B.; Liu, G.; Liashenko, A.; Piskorz, P.; Komaromi, I.; Gomperts, R.; Martin, R. L.; Fox, D. J.; Keith, T.; Al-Laham, M. A.; Peng, C. Y.; Nanayakkara, A.; Challacombe, M.; Gill, P. M. W.; Johnson, B.; Chen, W.; Wong, M. W.; Andres, J. L.; Gonzalez, C.; Head-Gordon, M.; Replogle, E. S.; Pople, J. A. *Gaussian98*, revision A.9; Gaussian, Inc.: Pittsburgh, PA, 1998.
(33) Oxgaard, J.; Wiest, O. *J. Phys. Chem. A* **2001**, *105*, 8236.
(34) Bigeleisen, J.; Mayer, M. G. *J. Chem. Phys.* **1947**, *15*, 261.
(35) Saunders, M.; Laidig, K. E.; Wolfsberg, M. *J. Am. Chem. Soc.* **1989**, *111*, 8989.
(36) Scott, A. P.; Radom, L. *J. Phys. Chem.* **1996**, *100*, 16502.
(37) Bell, R. P. *The Tunnel Effect in Chemistry*; Chapman & Hall: London, 1980; p 60.

An analogous reaction under identical conditions was taken to 78.9 ± 1.5% conversion.

NMR Measurements. NMR samples of standard and recovered material were in each case prepared identically by dissolving 2 g of indole in $CDCl_3$ to a level of 5 cm in a 10-mm NMR tube. A T_1 determination by the inversion−recovery method was carried out on each NMR sample. The ^{13}C spectra were recorded at 100.58 MHz with inverse-gated decoupling using inverse-gated decoupling with 80-s delays between calibrated 90° pulses. An acquisition time of 7.498 s was used and 206 272 points were collected. Integrations were determined numerically using a constant region for each peak that was ~5 times the peak width at half-height distance on either side of the peak. A zero-order baseline correction was generally applied, but in no case was a first-order (tilt) correction applied.

NMR Results. The integration of C4 of indole was set to 1000, and the average integrations for the other carbons for each reaction, along with the standard results for the starting materials, are shown in Table 2. For each sample, the total number of spectra obtained was eight. Table 2 also shows the values for R/R_0, calculated as the ratio of average integrations for recovered material relative to the standard. The standard deviations were calculated from eq 9. The isotope effects and errors shown in Table 2 and Figure 1 were then calculated as previously described.[30]

$$\Delta R/R0 = R/R0 * ((\Delta\text{IntSample/IntSample})2 + (\Delta\text{IntStandard/IntStandard})2)1/2 \quad (9)$$

Acknowledgment. D.A.S. and M.P.M. thank NIH grant # GM-45617 and The Robert A. Welch Foundation for support. O.W. and N.J.S. gratefully acknowledge support from NSF (CHE-9733050) and NIH (Grant CA73775) as well as the generous allocation of computing resources from the Office of Information Technology at the University of Notre Dame.

Supporting Information Available: Energies, zero point energies, imaginary frequencies, and Cartesian coordinates of all structures reported as well as a table of all computed isotope effects and a program for the numerical simulation of the isotope effects (PDF). This material is available free of charge via the Internet at http://pubs.acs.org.

JA026924Z